

## A model-based approach for the estimation of bearing forces and moments using outer-ring deformation

Kerst, Stijn; Shyrokau, Barys; Holweg, Edward

**DOI**

[10.1109/TIE.2019.2897510](https://doi.org/10.1109/TIE.2019.2897510)

**Publication date**

2019

**Document Version**

Accepted author manuscript

**Published in**

IEEE Transactions on Industrial Electronics

**Citation (APA)**

Kerst, S., Shyrokau, B., & Holweg, E. (2019). A model-based approach for the estimation of bearing forces and moments using outer-ring deformation. *IEEE Transactions on Industrial Electronics*, 67(1), 461-470. <https://doi.org/10.1109/TIE.2019.2897510>

**Important note**

To cite this publication, please use the final published version (if applicable). Please check the document version above.

**Copyright**

Other than for strictly personal use, it is not permitted to download, forward or distribute the text or part of it, without the consent of the author(s) and/or copyright holder(s), unless the work is under an open content license such as Creative Commons.

**Takedown policy**

Please contact us and provide details if you believe this document breaches copyrights. We will remove access to the work immediately and investigate your claim.

# A model-based approach for the estimation of bearing forces and moments using outer-ring deformation

Stijn Kerst, Barys Shyrokau, Edward Holweg

**Abstract**— Bearing load estimation would form a valuable addition to the fields of condition monitoring and system control. Despite effort spend on its development by all major bearing manufacturers no product solution has come to market yet. This can be attributed to both the complexity in conditioning of the strain measurement as well as its non-linearity with respect to the bearing loading. To address these issues, this paper proposes a novel approach based on modeling of the physical behavior of the bearing. An Extended Kalman Filter including a novel strain model is applied for signal conditioning whereas an Unscented Kalman Filter including a semi-analytical bearing model is proposed for reconstruction of the bearing load. An experimental study in both laboratory and field conditions shows that the proposed cascaded Kalman filtering approach leads to accurate estimates for all four considered bearings loads in various loading conditions. Besides an improvement on accuracy, the novel approach leads to a reduction in calibration effort.

**Index Terms**— Rolling Bearing, Condition monitoring, Load Reconstruction, Bearing modeling

## I. INTRODUCTION

Rolling bearings are essential components in a wide variety of products and machinery allowing for the rotational motion of shafts. As their failing is one of the most common reasons for machinery breakdown [1] bearing diagnosis and fault detection are active fields of research. This is reflected by the various condition monitoring approaches as vibration-, acoustic emission-, sound pressure-, lubrication- and thermal analysis that have been developed and applied [2-6].

Condition monitoring focuses on detection of incipient bearing failure or remaining useful life (RUL) estimation by detection of (local) bearing defects [7] in order to schedule upkeep or replacement. Excessive loading, bearing misalignment or improper loading are root causes for a considerable part of bearing defect initiation and growth. Bearing load monitoring would enable for the detection of these improper conditions and thereby allows for monitoring of the cause of defect initiation.

As bearings furthermore often form important connectivity points, load measurement could also provide valuable

information at system level. Of particular interest is the development of wheel-end load estimation as this would allow for improved vehicle dynamics control and safety systems such as load based- state estimation [8], anti-lock braking [9] and chassis control [10].

Hence it could serve as a valuable addition to condition monitoring as well as for system analysis and control. Due to these reasons all major bearing manufactures work on the development of the bearing upgrade to load-cell [11-16].

Load monitoring on a bearing level can be based on two different physical quantities. Either the outer-ring *deformation* is measured by the use of strain gauges [12, 17, 18], ultrasonic sensors [19] or optical fibers [20], or the relative inner- to outer-ring *displacement* is determined by hall effect [13, 21], eddy-current [22, 23] or capacitive [24] sensors. After signal conditioning, the measured physical quantities are translated to the bearing loading by empirical methods such as least squares fitting [12, 17] or artificial neural networks [25].

However, due to effects as strain lumping and thermal drift, current deformation based signal conditioning approaches are inapplicable for double row roller bearings as for instance found at vehicle wheel-ends. In this paper these difficulties are addressed and a novel conditioning approach to overcome these issues is proposed. The latter is the first of two main contributions of this paper, and encompasses a novel strain model and its implementation in an Extended Kalman Filter (EKF).

Besides the problem of conditioning itself, the non-linear relation between the conditioned signal and bearing loading is challenging to be effectively captured by the use of empirical methods. The latter is reflected by the case specific and/or partial solutions found for the load reconstruction phase [9, 12]. Although piecewise linearization [12] and higher order fitting [17] may lead to decent load estimates, the robustness and applicability of such approach for industrialization is debatable as it inevitably leads to numerous parameters subject to calibration. In order to capture the non-linear relationship and minimize calibration effort the second contribution of this paper is the introduction of a model based load reconstruction phase. The latter considers the implementation of a semi-analytical bearing model in an Unscented Kalman Filter (UKF).

The paper is structured as follows; in section II bearing strain, conditioning and its modeling are discussed. In section III the bearing load model is introduced. The implementation of the strain and load model in the Kalman Filter based

Manuscript received May 31, 2018; revised September 3 and October 1, 2018; accepted January 9, 2019.

Authors are with the Mechanical Engineering Department, Delft University of Technology, Delft, The Netherlands (e-mail: kerst@arrival.com, b.shyrokau@tudelft.nl, eholweg@vmi-group.com).

algorithm is presented in section IV. In section V the reference study is addressed. Section VI discusses the experimental setup after which the experimental results are presented and discussed in section VII. Finally, the conclusions and recommendations are presented in section VIII.

## II. BEARING STRAIN

An important aspect in bearing strain conditioning is the differentiation between bulk and local deformation. In this section both effects are elaborated and their signal conditioning methods are discussed. Finally the novel *strain model* is proposed which describes the relationship between the passing of loaded rolling elements and local outer-ring strain.

### A. Bulk and local deformation

The *bulk effect* or global deformation considers the average strain during a full passage of rolling elements as indicated in Fig. 1. It is directly affected by the applied bearing loading as well as by (pre-)stress due to thermal effects and boundary conditions. Its behavior is defined by bearing geometry, material properties and boundary conditions.

The *local effects* are contributed to the rolling element contact loads and their continuous rearrangement;

Considering equally spaced rolling elements by a cage the element rearrangement results in a periodic variation of load paths, stresses and strains for any bearing load. Any location on the outer-ring measuring the rolling element local contact deformation therefore will capture a cyclic strain for a running bearing. The location and properties of the strain measurement and local geometry determine the shape of the cyclic strain, of which an example is visualized in Fig. 1.

As depicted in Fig. 2 the sensitivity of the local strain to the local rolling element load is related to the rolling element load line or contact angle. Local geometry, material properties and the axial location of the measurement point define the magnitude and shape of the contact angle sensitivity.

In the case of a double row bearing with little axial spacing between both raceways any axially centered measurement location will capture a lumped measurement of both local in- and outboard strain effects. Assuming linear elastic mechanical behavior the superposition principle holds and hence the measured local strain is the sum of in- and outboard local effects as depicted in Fig. 3.

### B. Signal conditioning

The bulk effect can be determined by specific strain gauge design [12] or notch/low-pass filtering [9]. As thermal effects on the bulk deformation however are significant and hard to address, it provides an inaccurate measure for reconstruction of the bearing loading.

By the use of a peak-to-peak detection algorithm [11] the local strain amplitude can be determined. Although effective when a single raceway is considered, this approach is inapplicable for any lumped strain measurement (Fig. 3) as the amplitude of the super-positioned measurement is inconclusive; Asynchronicity of the in- and outboard rolling elements leads to varying phase differences which on its turn affects the measured local strain amplitude. Current

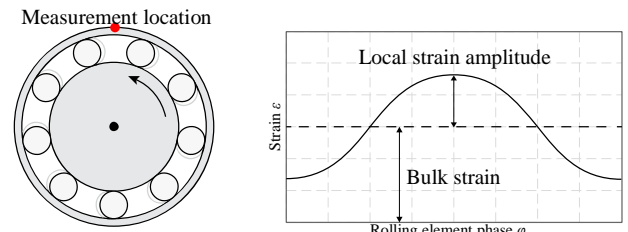


Fig. 1. Cyclic local strain behavior due to reallocation of rolling elements in a loaded running bearing

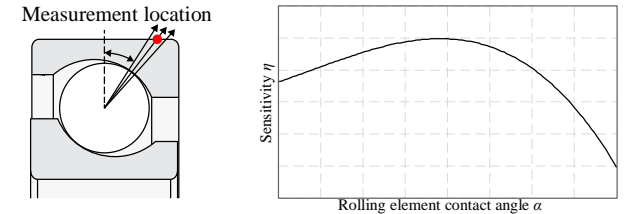


Fig. 2. Schematic representation of relationship between contact angle and measurement sensitivity  $\eta$

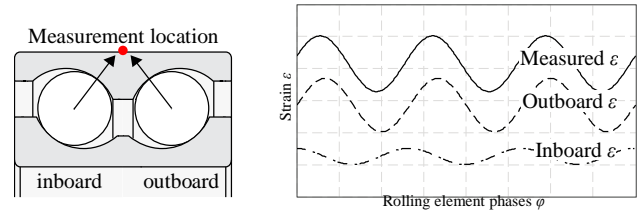


Fig. 3. Strain superposition of in- and outboard local strain effects

conditioning approaches furthermore are suboptimal with respect to noise suppression and signal bandwidth due to the basic signal processing involved.

To discriminate in- and outboard local effects and for improved signal quality a continuous model based tracing by the use of Kalman filtering is proposed. In the following the local strain model is proposed, which after implementation in the proposed algorithm is applied to determine the in- and outboard rolling element loads from local strain measurements.

### C. Local strain modeling equations

Based on the behavior discussed in subsection A the following general strain approximation model is proposed for the local strain resulting from a single loaded rolling element:

$$\varepsilon_l(\psi) = Q(\psi)G(\varphi)\eta(\alpha) \quad (1)$$

where  $\varepsilon_l$  is the outer-ring local strain at azimuth  $\psi$ ,  $Q$  is the rolling element load at azimuth  $\psi$ ,  $G$  is a normalized periodic transfer function dependent on the local rolling element phase  $\varphi$  and  $\eta$  represents the measurement location sensitivity as function of contact angle  $\alpha$ .

The periodic transfer function captures the effect of the changing load paths on the outer-ring local deformation. Assuming a constant rolling element load during the ball-passing period, the local strain variation can be fully addressed to the periodic transfer function. The following representation is proposed:

$$G(\varphi) = \sum_{n=1}^{N_h} a_n \cos(\varphi n + \phi_n) \quad (2)$$

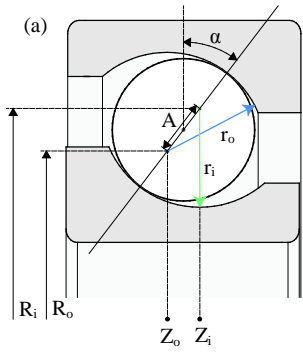


Fig. 4. Bearing section view showing bearing parameters

where  $a_n$  and  $\phi_n$  represent the magnitude and relative phase shifts of each of the  $n$  harmonics and  $N_h$  defines the number of harmonics considered. The local rolling element phase  $\varphi$  is periodic with  $-\pi \leq \varphi < \pi$  and equals 0 when an element is in line. Function normalization is achieved by setting the first harmonics' magnitude  $a_1$  to unity and phase  $\phi_1$  to zero.

Due to normalization of the periodic function the element load to strain magnitude is solely reflected by the measurement location sensitivity. For the sensitivity, which is a function of contact angle  $\alpha$ , the following polynomial description is proposed:

$$\eta(\alpha) = \sum_{n=0}^{N_p} c_n \alpha^n \quad (3)$$

where  $c_n$  are the polynomial coefficients and  $N_p$  is the order of the polynomial.

In case a double row bearing is considered the right-hand side of (1) can be extended by a similar description for the second raceway according to the superposition principle.

### III. BEARING LOAD MODEL

This section presents the *bearing load model* which relates the previously described in- and outboard rolling element loads to the bearing loading. As both real-time implementation and raceway deformation are considered important this study implements the semi-analytical model as introduced in [26]. In the following the bearing modeling equations are presented.

#### A. Modeling equations

The rolling element normal force  $Q$  at any azimuth angle  $\psi$  is described as a function of the local normal approach of both raceways:

$$Q(\psi) = K_n \delta(\psi)^{3/2} \quad (4)$$

where  $\delta$  is the raceway normal approach at azimuth  $\psi$  and  $K_n$  is the load-deflection factor. The inner-ring position and orientation are defined by 5 degrees of freedom. The outer-ring is modeled as flexible whilst its position is fixed. For any bearing azimuth angle  $\psi$  this results in the following description of normal approach  $\delta$  and contact angle  $\alpha$ :

$$\delta(\psi) = \left[ \left( R_i + \delta_x \cos(\psi) + \delta_y \sin(\psi) - (R_o + u_r(\psi)) \right)^2 + \left( Z_i + \delta_z + R_i \gamma_x \sin(\psi) + R_i \gamma_y \cos(\psi) - Z_o \right)^2 \right]^{1/2} - A \quad (5)$$

$$\alpha(\psi) = \tan^{-1} \left( \frac{(Z_i + \delta_z + R_i \gamma_x \sin(\psi) + R_i \gamma_y \cos(\psi) - Z_o)}{R_i + \delta_x \cos(\psi) + \delta_y \sin(\psi) - (R_o + u_r(\psi))} \right) \quad (6)$$

where  $R_i$ ,  $R_o$ ,  $Z_i$ ,  $Z_o$  and  $A$  are bearing geometry parameters as indicated in Fig. 4,  $\delta_x$ ,  $\delta_y$ ,  $\delta_z$  are the inner-ring translations in  $x$ ,  $y$  and  $z$  direction,  $\gamma_x$  and  $\gamma_y$  are the inner-ring rotations over  $x$ - and  $y$ -axis. Finally,  $u_r$  is the radial static elastic outer-raceway deformation. The latter is defined as:

$$u_r(\psi) = \mathbf{K}^{-1} \mathbf{Q} \quad (7)$$

where  $\mathbf{K}^{-1}$  is the outer-ring inverse stiffness matrix and  $\mathbf{Q}$  the vector of all rolling element loads. The inverse stiffness or compliance matrix represents the non-linear relationship between element loads and raceway deformation. In line with [26] the compliance matrix is approximated by:

$$\mathbf{K}^{-1} = \boldsymbol{\Phi}(\psi) \boldsymbol{\Theta}(\Psi) \quad (8)$$

where  $\boldsymbol{\Phi}(\psi)$  is a column vector of normalized orthogonal deformation shapes and  $\boldsymbol{\Theta}(\Psi)$  is a row vector of a Fourier-series based compliance approximation. The latter is determined by the use of a Finite Element study on the bearing outer-ring structure. For a detailed description of the race deformation modeling the reader is referred to [26].

The bearing forces and moments are calculated by summation of the rolling element load vector as follows:

$$\begin{aligned} F_{Bx} &= \sum_{n=1}^{N_{re}} Q(\psi_n) \cos(\alpha_n) \cos(\psi_n) \\ F_{By} &= \sum_{n=1}^{N_{re}} Q(\psi_n) \cos(\alpha_n) \sin(\psi_n) \\ F_{Bz} &= \sum_{n=1}^{N_{re}} Q(\psi_n) \sin(\alpha_n) \\ M_{Bx} &= \sum_{n=1}^{N_{re}} R_m Q(\psi_n) \sin(\alpha_n) \sin(\psi_n) \\ M_{By} &= \sum_{n=1}^{N_{re}} R_m Q(\psi_n) \sin(\alpha_n) \cos(\psi_n) \end{aligned} \quad (9)$$

where  $n$  represents the rolling element index,  $N_{re}$  is the number of rolling elements and  $R_m$  is the bearing pitch radius which equals  $(R_i + R_o)/2$ .

### IV. NOVEL LOAD ESTIMATION ALGORITHM

Using the modeling equations presented in previous sections a four-stage algorithm is proposed for the estimation of bearing loads based on strain measurement on the bearing outer-ring. The algorithm, shown in overview in Fig. 5, is characterized by two subsequent non-linear Kalman filters. The first filter, an Extended Kalman Filter, implements the strain model for translation of local strains to rolling element loads. The second Unscented Kalman Filter includes the bearing load model for translation of these element loads to the bearing state. The bearing state is then used for calculation of the bearing loading and to update the raceway deformation.

For computational efficiency the first filter is of the EKF type, whereas an UKF is applied in the second stage due to the high non-linearity of the model. Besides for simplified tuning

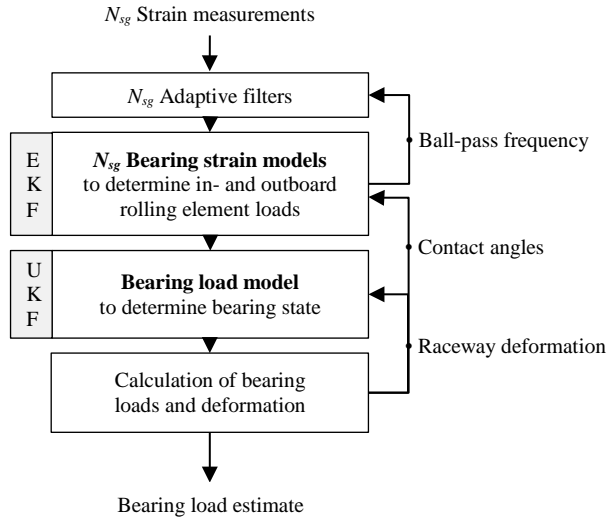


Fig. 5. Block diagram of the bearing load reconstruction algorithm

furthermore a cascaded approach is chosen as two independent physical phenomena without cross-covariance are described.

In the following a generalized description of the algorithm is provided assuming a double row bearing equipped with  $N_{sg}$  strain gauges.

#### A. Adaptive filtering

In this first stage of the algorithm all  $N_{sg}$  strain measurements are filtered to extract the local strain effects from the raw measurements. Adequate separation of bulk and local effects is only possible when the ball-pass frequency exceeds the bandwidth of the external load. The latter is considered either static and known or dynamic and related to the rotational frequency of the bearing. The local strain is extracted by the use of a 2<sup>nd</sup> order Butterworth high-pass filter with cutoff frequency  $f_c$  according to:

$$f_c = c_{bw} \bar{f}_{bw} \quad \text{if } \bar{f}_{bw} = \text{cons.} \quad (10)$$

$$f_c = c_{bp} f_{bp} \quad \text{if } \bar{f}_{bw} \neq \text{cons.} \quad (11)$$

where  $\bar{f}_{bw}$  is the upper frequency of the static bearing load bandwidth,  $f_{bp}$  is the ball-pass frequency estimate and  $c_{bw}$  ( $>1$ ) and  $c_{bp}$  ( $<1$ ) are tuning constants providing separation between bulk deformation and ball-pass frequencies. The case specific tuning constants should be chosen such that in operating conditions the high-pass filter provides respectively maximal and minimal attenuation of low and high frequency content such to maximize signal to noise ratio of the local strain.

Note that the separation of local strain from the raw measurement forms a fundamental requirement on the minimal bearing rotational speed.

#### B. Strain model based Extended Kalman Filter

The *strain model* is implemented in a parallel EKF approach to estimate local in- and outboard rolling element loads, phases and frequencies from the  $N_{sg}$  local strain measurements. For each local strain signal a separate filter is set up according to the description as follows.

The EKF system equations are defined as:

$$\begin{aligned} \mathbf{x}_{n,k} &= \mathbf{F} \mathbf{x}_{n,k-1} + \mathbf{w}_n \\ \mathbf{y}_{n,k} &= f(\mathbf{x}_{n,k}, \mathbf{u}_{n,k}) + \mathbf{v}_n \end{aligned} \quad (12)$$

#### EXTENDED KALMAN FILTER EQUATIONS

##### Initialization

$$\hat{\mathbf{x}}_{n,0} = E[\mathbf{x}_n]$$

$$\mathbf{P}_{n,0} = E[(\mathbf{x}_n - \hat{\mathbf{x}}_{n,0})(\mathbf{x}_n - \hat{\mathbf{x}}_{n,0})^T]$$

##### 1. Time update

$$\hat{\mathbf{x}}_{n,k}^- = \mathbf{F} \hat{\mathbf{x}}_{n,k-1}$$

$$\mathbf{P}_{n,k}^- = \mathbf{F} \mathbf{P}_{n,k-1} \mathbf{F}^T + \mathbf{Q}_{n,k}$$

##### 2. Measurement update

$$\mathbf{K}_{n,k} = \mathbf{P}_{n,k}^- \mathbf{H}_{n,k}^T (\mathbf{H}_{n,k} \mathbf{P}_{n,k}^- \mathbf{H}_{n,k}^T + \mathbf{R}_{n,k})^{-1}$$

$$\hat{\mathbf{x}}_{n,k} = \hat{\mathbf{x}}_{n,k}^- + \mathbf{K}_{n,k} (\mathbf{y}_{n,k} - f(\hat{\mathbf{x}}_{n,k}^-, \mathbf{u}_{n,k}))$$

$$\mathbf{P}_{n,k} = \mathbf{P}_{n,k}^- - \mathbf{K}_{n,k} \mathbf{H}_{n,k} \mathbf{P}_{n,k}^-$$

where  $\mathbf{H}_{n,k} = \partial f(\hat{\mathbf{x}}_{n,k}^-) / \partial \hat{\mathbf{x}}_{n,k}^-$ , which is the linearization of the output equation at the current state estimate.

where  $\mathbf{x}_n$  and  $\mathbf{y}_n$  are respectively the state and measurement vector of the  $n^{\text{th}}$  filter,  $\mathbf{F}$  is the linear process model,  $f$  is the non-linear measurement model,  $\mathbf{u}_n$  is the external input vector and  $\mathbf{w}_n$  and  $\mathbf{v}_n$  are the  $n^{\text{th}}$  filter process and measurement noise matrixes respectively, which are assumed as zero-mean Gaussian white noise with covariance  $\mathbf{Q}_n$  and  $\mathbf{R}_n$ . The state, measurement and external input vector are defined as:

$$\mathbf{x}_{n,k} = [\omega_{n,i,k} \quad \varphi_{n,i,k} \quad Q_{n,i,k} \quad \omega_{n,o,k} \quad \varphi_{n,o,k} \quad Q_{n,o,k}]^T \quad (13)$$

$$\mathbf{y}_{n,k} = [\varepsilon_{n,l,k} \quad \bar{\omega}_{i,k} \quad \bar{\omega}_{o,k}]^T \quad (14)$$

$$\mathbf{u}_{n,k} = [\alpha_{n,i,k} \quad \alpha_{n,o,k}]^T \quad (15)$$

where  $\omega$  is the ball-pass frequency,  $\varepsilon_{n,l}$  is the local strain determined by the adaptive filtering phase,  $\bar{\omega}_i$  and  $\bar{\omega}_o$  are pseudo measurements of the ball-pass frequency, and  $\alpha_{n,i}$  and  $\alpha_{n,o}$  are the rolling element contact angles obtained from the bearing load calculation stage. The  $i$  and  $o$  subscripts refer to in- and outboard effects respectively.

The ball-pass frequency pseudo measurements are added to avoid observability issues during low excitation of the respective raceways and equal the current most trusted estimated ball-pass frequency. The linear process model  $\mathbf{F}$  is defined as the identity matrix with two off-diagonal terms on (2,1) and (5,4) equaling  $1/t_s$ , where  $t_s$  is the sampling period, to increment in- and outboard phases with the current respective rotational frequency estimates.

#### C. Load model based Unscented Kalman Filter

The *bearing load model* is implemented in an UKF to estimate the bearing state based on the estimated rolling element loads. The UKF system equations are defined as follows:

$$\mathbf{x}_{b,k} = \mathbf{x}_{b,k-1} + \mathbf{w}_b \quad (16)$$

$$\mathbf{y}_{b,k} = g(\mathbf{x}_{b,k}, \mathbf{u}_{b,k}) + \mathbf{v}_b$$

where  $\mathbf{x}_b$  is the state vector,  $\mathbf{y}_b$  is the measurement vector,  $g$  is the non-linear measurement model,  $\mathbf{u}_b$  is the external input vector and  $\mathbf{w}_b$  and  $\mathbf{v}_b$  are the process and measurement noise which are assumed to be zero-mean Gaussian white noise with covariance of respectively  $\mathbf{Q}_b$  and  $\mathbf{R}_b$ . Note that no process

UNSCENTED KALMAN FILTER EQUATIONS

Initialization

$$\begin{aligned}\hat{\mathbf{x}}_{b,0} &= E[\mathbf{x}_b] \\ \mathbf{P}_{b,0} &= E[(\mathbf{x}_b - \hat{\mathbf{x}}_{b,0})(\mathbf{x}_b - \hat{\mathbf{x}}_{b,0})^T] \\ W_0^c &= \lambda / (L + \lambda) + (1 - \alpha^2 + \beta) \\ W_i^c &= 1 / (2(L + \lambda)) \quad i = 1, \dots, 2L\end{aligned}$$

1. Time update

$$\begin{aligned}\hat{\mathbf{x}}_{b,k}^- &= \hat{\mathbf{x}}_{b,k-1} \\ \mathbf{P}_{b,k}^- &= \mathbf{P}_{b,k-1} + \mathbf{Q}_{b,k} \\ \mathbf{X}_{b,k}^- &= \begin{bmatrix} \hat{\mathbf{x}}_{b,k}^- & \hat{\mathbf{x}}_{b,k}^- + \gamma \sqrt{\mathbf{P}_{b,k}^-} & \hat{\mathbf{x}}_{b,k}^- - \gamma \sqrt{\mathbf{P}_{b,k}^-} \end{bmatrix} \\ \mathbf{Y}_{b,k}^- &= g(\mathbf{X}_{b,k}^-, \mathbf{u}_{b,k}) \\ \hat{\mathbf{y}}_{b,k}^- &= g(\hat{\mathbf{x}}_{b,k}^-, \mathbf{u}_{b,k})\end{aligned}$$

2. Measurement update

$$\begin{aligned}\mathbf{P}_{\hat{\mathbf{y}}_{b,k}, \hat{\mathbf{y}}_{b,k}} &= \sum_{i=0}^{2L} W_i^c (\mathbf{Y}_{b,k}^- - \hat{\mathbf{y}}_{b,k}^-) (\mathbf{Y}_{b,k}^- - \hat{\mathbf{y}}_{b,k}^-)^T + \mathbf{R}_{b,k} \\ \mathbf{P}_{\hat{\mathbf{x}}_{b,k}, \hat{\mathbf{y}}_{b,k}} &= \sum_{i=0}^{2L} W_i^c (\mathbf{X}_{b,k}^- - \hat{\mathbf{x}}_{b,k}^-) (\mathbf{Y}_{b,k}^- - \hat{\mathbf{y}}_{b,k}^-)^T \\ \mathbf{K}_{b,k} &= \mathbf{P}_{\hat{\mathbf{x}}_{b,k}, \hat{\mathbf{y}}_{b,k}} \mathbf{P}_{\hat{\mathbf{y}}_{b,k}, \hat{\mathbf{y}}_{b,k}}^{-1} \\ \hat{\mathbf{x}}_{b,k} &= \hat{\mathbf{x}}_{b,k}^- + \mathbf{K}_{b,k} (\mathbf{y}_{b,k} - \hat{\mathbf{y}}_{b,k}^-) \\ \mathbf{P}_{b,k} &= \mathbf{P}_{b,k}^- - \mathbf{K}_{b,k} \mathbf{P}_{\hat{\mathbf{y}}_{b,k}, \hat{\mathbf{y}}_{b,k}} \mathbf{K}_{b,k}^T\end{aligned}$$

where  $\alpha$  and  $\beta$  control the sigma point spread,  $L$  is the length of the state vector and  $\lambda$  is defined as  $\lambda = \alpha^2 L - L$ .

model is described as it equals the identity matrix. The state, measurement and external input vector are defined as:

$$\mathbf{x}_b = [\delta_x \quad \delta_y \quad \delta_z \quad \gamma_x \quad \gamma_y]^T \quad (17)$$

$$\mathbf{y}_b = [\delta_{i,1} \quad \delta_{o,1} \quad \dots \quad \delta_{i,N_{sg}} \quad \delta_{o,N_{sg}}]^T \quad (18)$$

$$\mathbf{u}_b = [u_r(\psi_1) \quad \dots \quad u_r(\psi_{N_{sg}})]^T \quad (19)$$

where the measurement vector consists of the normal approaches calculated using the previously estimated rolling element loads by (4). This transformation is applied as this leads to a better convergence of the bearing model due to the nature of (4) that results in a discontinuity in the calculated element load. The raceway deformation is regarded as external input and is obtained from the subsequent bearing model calculation phase.

D. Calculation of bearing load and deformation

Using the UKF state vector and (4-9) all rolling element loads, contact angles and subsequent bearing loads can be calculated based on the current raceway deformation estimate. The calculated rolling element loads are then used for updating the deformation estimate by (7-8).

V. REFERENCE LOAD ESTIMATION ALGORITHM

The results of the novel estimation approach are assessed by a comparison study to a state-of-the-art bulk deformation – coefficient based load estimation algorithm by combining

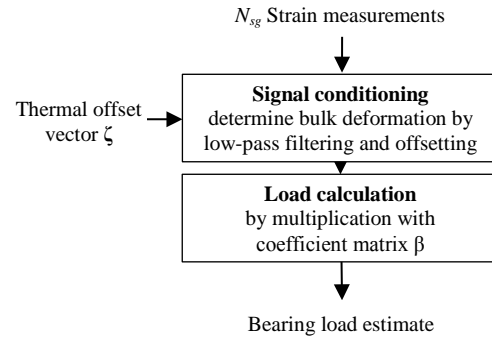


Fig. 6. Block diagram of the reference load estimation algorithm

features of [12, 17]. The algorithm, shown in overview in Fig. 6, applies a 2<sup>nd</sup> order Butterworth low-pass filter with a cutoff frequency of 10 Hz to determine the bulk deformation. After offsetting the filtered measurements by the use of thermal offset vector  $\zeta$ , the bearing loads are calculated:

$$\mathbf{y}_r = \mathbf{x}_r \boldsymbol{\beta} + \mathbf{v}_r \quad (20)$$

where  $\mathbf{y}_r$  is the vector of bearing load estimates,  $\mathbf{x}_r$  is the deformation vector,  $\boldsymbol{\beta}$  is the coefficient matrix and  $\mathbf{v}_r$  is the noise term. The deformation vector  $\mathbf{x}_r$  is defined as:

$$\mathbf{x}_r = [\varepsilon_{b,1} \quad \dots \quad \varepsilon_{b,N_{sg}} \quad \varepsilon_{b,1}^2 \quad \dots \quad \varepsilon_{b,N_{sg}}^2] \quad (21)$$

where  $\varepsilon_b$  is the outer-ring bulk deformation offsetted by offset vector  $\zeta$ . The latter is applied to compensate for thermal drift of the bulk deformation.

VI. EXPERIMENTAL SETUP

A. Bearing instrumentation

The outer-ring of a BMW 5-series front wheel-end bearing is instrumented with four ( $N_{sg}=4$ ) general-purpose strain gauges at a 90 degree interval over the bearing circumference. The gauges are placed in line with the principal axis of the bearing as the study aims to estimate radial forces and moments over these two axis. Due to the tight axial raceway spacing each strain gauge considers a lumped in- and outboard strain measurement. The strain gauges, specified in Table I, are applied in a Wheatstone bridge setup and amplified using an Peekel 9236 type conditioner. A layer of silicone is applied to protect the strain gauges and wiring from the harsh wheel-end environment. Fig. 7 shows the instrumented bearing before mounting.

B. Laboratory and field test setup

A dedicated bearing test rig is used for testing in laboratory conditions. The test rig, shown in Fig. 8, allows for dynamic loading of all 5 relevant degrees of freedom by the use of force controlled hydraulic actuators while rotating the bearing with an electric motor. Besides the instrumented bearing the setup includes the steering knuckle to more closely resemble vehicle implementation. Data acquisition is performed by the use of a Yokogawa DL750P mixed signal oscilloscope at a sampling rate of 2 kHz.

The field tests are performed on a BMW-5 series E60 type production vehicle at an old airstrip. The test vehicle, shown

TABLE I  
STRAIN GAUGE SPECIFICATIONS

Type	CEA-06-062UR-350	Pattern Type	Rectangular Rosette
Strain range	±3%	Active length	1.57 mm
Resistance	350 Ohms	Active width	1.57 mm
Gauge factor	2.150 ± 0.5%	Operating temp.	-75~175°C

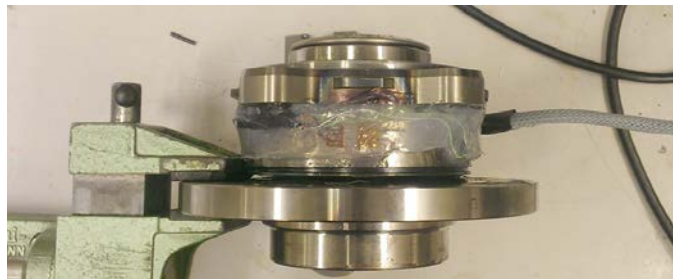


Fig. 7. The instrumented bearing before mounting on the test setup

in Fig. 9, is equipped with a VELOS wheel force transducer [27] that serves as reference load measurement. Data acquisition is performed by the use of a dSpace Autobox at a sampling rate of 500 Hz.

The algorithm is implemented in Matlab/Simulink and applied off-line on the data acquired during experiments on both test setups.

### C. Experimental study

The presented results consider two load cases on the bearing test system and one on the test vehicle. All tested loading conditions consider realistic wheel-end bearing loads.

For each load case a qualitative and quantitative analysis based on time domain results and root-mean-square error (RMSE) is provided. The RMSE results are provided in both absolute and relative terms, where the latter is related to the full experimental excitation range as indicated in Table II.

The load cases are evaluated on the estimation accuracy of longitudinal force  $F_x$ , vertical force  $F_z$ , tilting moment  $M_x$  and self-aligning moment  $M_z$  according to the sign convention as indicated in Fig. 9. Lateral force  $F_y$  is omitted as it was found that the setup with only four strain gauges provides insufficient information for accurate estimation.

The laboratory and field data results are filtered using a 2<sup>nd</sup> order Butterworth low pass filter with cutoff frequencies of respectively 4 and 1 Hz.

### D. Parameter definition & calibration

As the *bearing load model* is a well-established and validated modeling part its parameters are defined a priori such to minimize calibration effort. By the use of technical drawings the geometrical parameters are defined whilst the bearing compliance is determined by a Finite Element study in line with [26].

Quantification of the introduced *strain model* parameters is achieved by the use of a calibration routine. The order of the periodic transfer function and sensitivity polynomial are set to  $N_h = 2$  and  $N_p = 3$  respectively. As the bearing is plane symmetric, the front and rear strain model parameters are considered to be equal, resulting in a total of 18 parameters for calibration.

The parameters are calibrated by a non-linear least squares minimization procedure of the radial forces and accompanying

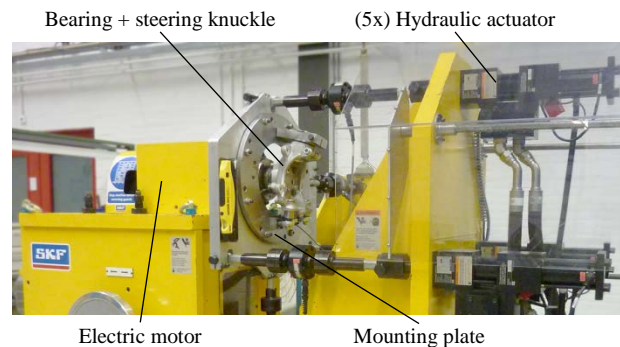


Fig. 8. The bearing test system located at our industrial partner



Fig. 9. The instrumented test vehicle including load sign convention

TABLE II  
TOTAL COMBINED EXCITATION RANGE  
OF CALIBRATION AND VALIDATION EXPERIMENTS

Load		Min	Max
Longitudinal force	$F_x$	-5.5 kN	0.5 kN
Vertical force	$F_z$	1.5 kN	10.0 kN
Tilting moment	$M_x$	-0.7 kNm	2.1 kNm
Self-aligning moment	$M_z$	-0.4 kNm	0.2 kNm

moments based on a total of 166 seconds of test rig experiments containing various road realistic load cases. In line with common practice, none of the presented load cases in the results section are in the calibration set.

### E. Algorithm initialization & tuning

For initialization of the algorithm only the initial rotational frequency is required as prior knowledge. In the experimental setup this is obtained from the wheel speed encoders; however, this could also be estimated based on the raw strain signals using a frequency estimator.

As common in the application of Kalman filtering, the process and measurement noise covariance matrixes are tuned for improved convergence and robustness of the nonlinear filters. As the strain gauge excitation varies significantly, a rule based tuning is applied based on internal filter states.

### F. Reference study setup

The 32 coefficients in matrix  $\beta$  are determined by a multivariate linear least squares regression analysis using the same 166 seconds of test rig experiments as used for calibration of the proposed algorithm. The thermal offset vector  $\zeta$  for compensation of thermal drift is re-calibrated on a regular basis during unloaded conditions (test rig, every 5 min) and lifting of the wheel (test vehicle, every half an hour) to avoid large estimation errors.

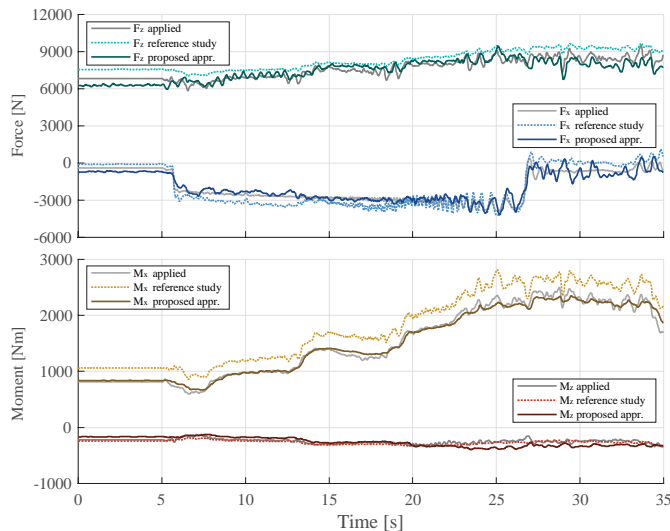


Fig. 10. Time domain results of load case 1 performed on the bearing test rig

TABLE III  
RMSE OF LOAD CASE 1

Load		Reference study		Proposed approach	
Longitudinal force	$F_x$	529 N	8.8 %	375 N	6.3 %
Vertical force	$F_z$	725 N	8.5 %	439 N	5.2 %
Tilting moment	$M_x$	290 Nm	10.4 %	64 Nm	2.3 %
Self-aligning moment	$M_z$	30 Nm	4.9 %	64 Nm	10.7 %

## VII. EXPERIMENTAL RESULTS AND DISCUSSION

In this section the three experiments are presented, followed by an overall discussion in subsection D.

### A. Test rig: Cornering and braking combined loading

This first load case considers the bearing loads during cornering and braking to analyze the estimation results for combined loading. The experiment is performed on the bearing test rig at a constant rotational speed of 1000 rpm, resembling a driving speed of approximately 120 km/h. The time domain results and quantitative evaluation are presented in Fig. 10 and Table III respectively.

The time domain results show good quasi-static tracking of all loads determined by the proposed approach whereas significant errors on both forces and tilting moment  $M_x$  are noted for the reference study. The results furthermore show that the precision of the longitudinal force  $F_x$  by the proposed approach decreases as overall bearing loading increases.

The RMSE results confirm that the proposed approach outperforms the reference study on all loads except for the low excited self-aligning moment  $M_z$ .

### B. Test rig: Slalom maneuver

The second load case regards the loading during a slalom maneuver to analyze the estimation quality for large internal load variations. The test is performed at a constant rotational speed of 1000 rpm. Fig. 11 shows the load case results over time for vertical force  $F_z$  and tilting moment  $M_x$  as well as the indication of the time domain used for the quantitative results presented in Table IV.

From the time domain results different regions in estimation quality can be observed for the proposed approach; during the

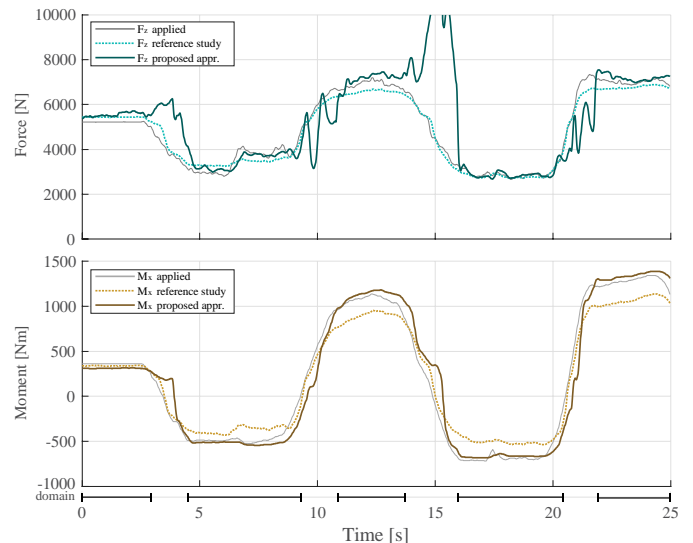


Fig. 11. Time domain results of load case 2 performed on the bearing test rig including the domain indication for the quantitative results of table IV

TABLE IV  
RMSE OF INDICATED TIME DOMAIN LOAD CASE 2

Load		Reference study		Proposed approach	
Longitudinal force	$F_x$	197 N	3.3 %	473 N	7.9 %
Vertical force	$F_z$	269 N	3.2 %	275 N	3.2 %
Tilting moment	$M_x$	155 Nm	5.5 %	68 Nm	2.4 %
Self-aligning moment	$M_z$	42 Nm	7.0 %	22 Nm	3.6 %

application of tilting moment  $M_x$  a good tracking is observed whilst large errors are encountered in the switching periods in-between. The erroneous periods, which are related to difficulties in the EKF strain filters, are addressed in the discussion section.

It is noted that the bulk deformation based reference study is not affected during the in-/outboard switching periods. However, an underestimation of tilting moment  $M_x$  is encountered in cornering conditions.

The quantitative results, focused only on the stable estimation domain, show similar performance of the proposed algorithm to load case 1. The reference study performs considerably better with respect to load case 1.

### C. Test vehicle: Cornering

This last load case considers a cornering maneuver on the test vehicle. The test is performed at a slowly increasing driving speed from 35 km/h to 60 km/h whilst a constant cornering radius of approximately 50 m is maintained. Time and quantitative results of this 100 second long experiment are presented in Fig. 12 and Table V respectively.

Time domain results show good quasi-static load estimates by the proposed approach, although a slight underestimation of the vertical force  $F_z$  is observed. The reference study on the other hand shows considerable errors for all load estimates except self-aligning moment  $M_z$ . In line with load case 1, precision of the longitudinal force estimate  $F_x$  decreases as overall bearing loading increases.

The quantitative results confirm these observations as errors of the proposed approach are in line with load case 1 and 2, whilst a considerable increase in RMS errors of longitudinal

force  $F_x$ , vertical force  $F_z$  and tilting moment  $M_x$  for the reference study is noted.

#### D. Discussion

The *proposed approach* leads an accurate estimation of all four considered loads in both laboratory as well as field conditions.

Only during switching of moment direction erroneous load estimates are noted. These errors originate from the conditioning phase of the algorithm as the EKF has difficulties in discriminating the super-positioned strains during the in-/outboard rolling element load transfer. This discrimination is made difficult as states change quickly whilst the amount of information is limited due to the low bearing loading and consequent deformation. However, the Kalman filter recovers after switching of moment direction showing the overall robustness of the approach.

The decrease of precision of the low-excited longitudinal force estimate  $F_x$  during load case 1 and 3 is attributed to cross-coupling as the rolling element load distribution is dependent on all 5 bearing loads whilst strain gauge locations are fixed. Due to the former any individual load can be reflected by various rolling element load distributions. The latter consequently results in a varying sensitivity and precision depending on this load distribution.

The offset in vertical force estimate  $F_z$  during the field test is attributed to minor differences in boundary conditions with respect to the laboratory setup.

The *reference study* shows large errors in the estimation of longitudinal force  $F_x$ , vertical force  $F_z$  and the over-turning moment  $M_x$ . The origin of these errors is twofold. The constant biases on vertical force  $F_z$  and tilting moment  $M_x$  during load case 1 and 3 are attributed to thermal effects. The varying estimation errors, as the underestimation of tilting moment  $M_x$  in load case 2 and varying under- and overestimation of longitudinal force  $F_x$  during load case 1 and 3, on the other hand find their origin in the coefficient based load calculation.

Overall it is observed that for both methods moments are more accurately estimated than forces. This is a consequence of the relatively larger bulk and local deformation resulting from moment loading.

It can be noted that, even with regular recalibration of thermal offset vector  $\zeta$ , thermal drift is the weak point of the bulk deformation based conditioning of the reference study. Due to conditioning focused on local strain the proposed algorithm is invariant to these thermal effects resulting in better estimates and a good repeatability.

Focusing on the load reconstruction phase, omitting thermal effects, one could conclude that the model based load reconstruction leads to only a minor increase in estimation accuracy. However, the main advantages of the application of a model based approach with respect to a data-driven method are in calibration and its robustness. Due to modeling and usage of bearing physical parameters the number of parameters subject to calibration is reduced. As principal relationships are furthermore defined a priori the risk of overfitting decreases and calibration effort is reduced.

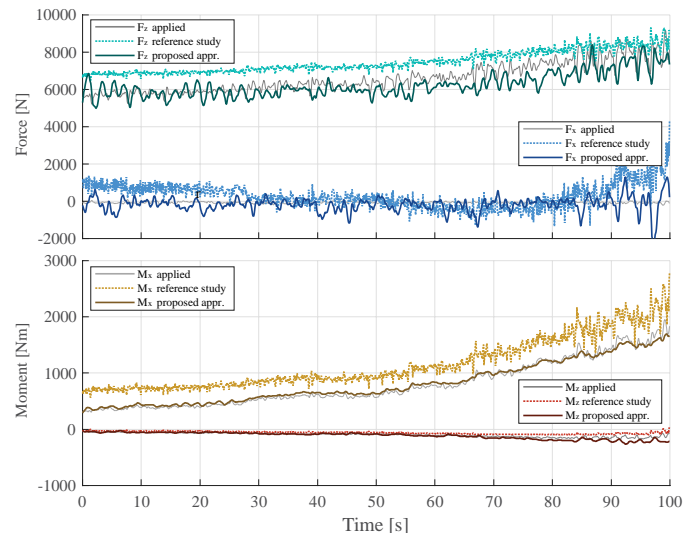


Fig. 12. Time domain results of load case 3 performed on the test vehicle

TABLE V  
RMSE OF LOAD CASE 3

Load		Reference study	Proposed approach
Longitudinal force	$F_x$	711 N 11.9 %	416 N 6.9 %
Vertical force	$F_z$	897 N 10.6 %	624 N 7.3 %
Tilting moment	$M_x$	356 Nm 12.7 %	77 Nm 2.8 %
Self-aligning moment	$M_z$	41 Nm 6.8 %	34 Nm 5.7 %

#### VIII. CONCLUSION AND RECOMMENDATIONS

This paper presents a novel model based strain conditioning and load calculation phase for the purpose of bearing load estimation. A cascaded Extended and Unscented Kalman filtering approach including a novel strain model and semi-analytical bearing model is proposed. An experimental study covering both laboratory and field tests shows that the novel approach leads to accurate load estimates in various conditions and outperforms the reference study. Of particular interest are the relatively low RMS errors of 6.9% and 7.3% for longitudinal force  $F_x$  and vertical force  $F_z$  and 2.8% and 5.7% for tilting moment  $M_x$  and self-aligning moment  $M_z$  obtained during the field tests whilst calibration was conducted in laboratory conditions only. The results show that the proposed local strain based conditioning approach is invariant to thermal effects and leads to a good repeatability. The model based load reconstruction phase of the algorithm furthermore improves accuracy whilst the risk of overfitting decreases and calibration effort is reduced.

Future work should focus on achieving an accurate and robust load estimate over the full (case specific) excitation range for any considered bearing. Of particular interest is the effect of the amount and location of strain gauges with respect to the estimation accuracy. Next to that a substantial improvement could be achieved by bearing shape optimization specifically for load estimation.

#### REFERENCES

[1] T. Williams, X. Ribadeneira, S. Billington, and T. Kurfess, "Rolling element bearing diagnostics in run-to-failure lifetime

testing," *Mechanical Systems and Signal Processing*, vol. 15, pp. 979-993, 2001.

[2] N. Tandon and A. Choudhury, "A review of vibration and acoustic measurement methods for the detection of defects in rolling element bearings," *Tribology international*, vol. 32, pp. 469-480, 1999.

[3] I. El-Thalji and E. Jantunen, "A summary of fault modelling and predictive health monitoring of rolling element bearings," *Mechanical Systems and Signal Processing*, vol. 60-61, pp. 252-272, 2015.

[4] H. de Azevedo, A. Araújo, and N. Bouchonneau, "A review of wind turbine bearing condition monitoring: State of the art and challenges," *Renewable and Sustainable Energy Reviews*, vol. 56, pp. 368-379, 2016.

[5] J. Lee, F. Wu, W. Zhao, M. Ghaffari, L. Liao, and D. Siegel, "Prognostics and health management design for rotary machinery systems—Reviews, methodology and applications," *Mechanical Systems and Signal Processing*, vol. 42, pp. 314-334, 2014.

[6] J. Sun, C. Yan, and J. Wen, "Intelligent Bearing Fault Diagnosis Method Combining Compressed Data Acquisition and Deep Learning," *IEEE Transactions on Instrumentation and Measurement*, vol. 67, pp. 185-195, 2018.

[7] T. Liu and J. Mengel, "Intelligent monitoring of ball bearing conditions," *Mechanical Systems and Signal Processing*, vol. 6, pp. 419-431, 1992.

[8] K. Nam, S. Oh, H. Fujimoto, and Y. Hori, "Estimation of sideslip and roll angles of electric vehicles using lateral tire force sensors through RLS and Kalman filter approaches," *IEEE Transactions on Industrial Electronics*, vol. 60, pp. 988-1000, 2013.

[9] S. Kerst, B. Shyrokau, and E. Holweg, "Anti-lock Braking Control based on Bearing Load Sensing," in *EuroBrake*, Dresden, Germany, 2015, pp. 4-10.

[10] M. Gerard, "Global chassis control and braking control using tyre forces measurement," PhD thesis, Delft University of Technology, 2011.

[11] H. Mol, "Method and sensor arrangement for load measurement on rolling element bearing based on model deformation," U.S. Patent 7389701, 2008.

[12] K. Nishikawa, "Hub Bearing with Integrated Multi-axis Load Sensor," *Technical Review*, 2011.

[13] K. Ono, T. Takizawa, and M. Aoki, "Preload measuring device for double row rolling bearing unit," U.S. Patent 8864382, 2014.

[14] H. van der Knokke, R. Wunderlich, K. Hauser, and R. Hollweck, "Force-sensing bearing," U.S. Patent 7316168, 2008.

[15] M. Kraus and M. Bäuml, "Continuous wheel force measurement for passenger vehicles and commercial vehicles," in *6th International Munich Chassis Symposium*, Munich, Germany, 2015, pp. 717-717.

[16] M. Baeuml, F. Dobre, H. Hochmuth, M. Kraus, H. Krehmer, R. Langer, et al., "The Chassis of the Future," in *Schaeffler Seminar*, 2014.

[17] S. Kerst, B. Shyrokau, and E. Holweg, "Reconstruction of Wheel Forces Using an Intelligent Bearing," *SAE International Journal of Passenger Cars-Electronic and Electrical Systems*, vol. 9, pp. 196-203, 2016.

[18] S. Kerst, B. Shyrokau, and E. Holweg, "Wheel force measurement for vehicle dynamics control using an intelligent bearing," in *Advanced Vehicle Control*, 2016, pp. 547-552.

[19] W. Chen, R. Mills, and R. Dwyer-Joyce, "Direct load monitoring of rolling bearing contacts using ultrasonic time of flight," *Proc. R. Soc. A*, vol. 471, p. 20150103, 2015.

[20] A. Reedman and H. Yang, "Bearing monitoring using a fibre bragg grating," U.S. Patent 8790013, 2014.

[21] K. Nam, "Application of novel lateral tire force sensors to vehicle parameter estimation of electric vehicles," *Sensors*, vol. 15, pp. 28385-28401, 2015.

[22] H. A. Mol, S. Van Ballegooij, and J. M. Storcken, "Load determining system for a rolling element bearing," U.S. Patent Application 15/533,545, 2016.

[23] K. Ayandokun, P. Orton, N. Sherkat, and P. Thomas, "Smart bearings: developing a new technique for the condition monitoring of rotating machinery," in *IEEE Int. Conference on Intelligent Engineering Systems*, 1997, pp. 505-510.

[24] L. Rasolofondraibe, B. Pottier, P. Marconnet, and X. Chiementin, "Capacitive sensor device for measuring loads on bearings," *IEEE Sensors Journal*, vol. 12, pp. 2186-2191, 2012.

[25] B. Leeuwen and J. Zuurbier, "Vehicle state estimation based on load sensing," presented at the Vehicle Dynamics Expo, 2007.

[26] S. Kerst, B. Shyrokau, and E. Holweg, "A semi-analytical bearing model considering outer race flexibility for model based bearing load monitoring," *Mechanical Systems and Signal Processing*, vol. 104, pp. 384-397, 2018.

[27] A. Rupp, V. Grubisic, and J. Neugebauer, "Development of a multi-component wheel force transducer—a tool to support vehicle design and validation," SAE Technical Paper 0148-7191, 1993.



previously at SKF and currently at Arrival in London.

**Stijn Kerst** was born in Raamsdonk, the Netherlands, in 1986. He received the B.Sc. degree in Industrial Design Engineering and M.Sc. degree in Mechanical Engineering from Delft University of Technology, Delft, the Netherlands, in 2009 and 2012 respectively. He is currently working towards the Ph.D. degree in Mechanical Engineering at Delft University of Technology on the topic of bearing load measurement. Additionally he is working on the valorisation of his research in industry;



vehicle dynamics and control, motion comfort and driving simulator technology. Scholarship and award holder of FISITA, DAAD, SINGA, ISTVS and CADLM.

**Barys Shyrokau** was born in Barysaw, Belarus, in 1981. He received the DiplEng degree (cum laude), 2004 in Mechanical Engineering from the Belarusian National Technical University, and the joint PhD degree, 2015 in Control Engineering from Nanyang Technological University and Technical University Munich. He is assistant professor in the Section of Intelligent Vehicles, Department of Cognitive Robotics, at Delft University of Technology and involved in research related to



dynamics and control, motion comfort and driving simulator technology. Currently he is working as COO for the VMI Group, based in the Netherlands.

**Edward Holweg** was born in Maassluis, the Netherlands, in 1967. He received his M.Sc. degree in Electrical Engineering in 1990 and PhD degree in 1996 from the Delft University of Technology, the Netherlands. He has been working (2008-2017) as part-time full professor at the Faculty of 3ME (Mechanical, Maritime and Materials Engineering), at the Delft University of Technology, the Netherlands, in the area of Intelligent Automotive Systems and involved in research related to vehicle